Research Square

Preprints are preliminary reports that have not undergone peer review.
They should not be considered conclusive, used to inform clinical practice,
or referenced by the media as validated information.

European Electricity Grids May Exhibit Heatwave-induced Capacity Bottlenecks

Srinivasan Keshav

sk818@cam.ac.uk

University of Cambridge

Minghua Chen

City University, Hong Kong

Enming Liang

City University of Hong Kong

Article

Keywords:

Posted Date: October 30th, 2024

DOI: https://doi.org/10.21203/rs.3.rs-5333852/v1

License: This work is licensed under a Creative Commons Attribution 4.0 International License.
Read Full License

Additional Declarations: There is **NO** Competing Interest.

Version of Record: A version of this preprint was published at Nature Energy on October 22nd, 2026. See the published version at https://doi.org/10.1038/s41560-026-02151-1.

European Electricity Grids May Exhibit Heatwave-induced Capacity Bottlenecks

Enming Liang[1], Minghua Chen[1*], Srinivasan Keshav[2*]

[1]Department of Data Science, City University of Hong Kong.
[2]Department of Computer Science and Technology, University of Cambridge.

*Corresponding author(s). E-mail(s): minghua.chen@cityu.edu.hk; sk818@cam.ac.uk;
Contributing authors: eliang4-c@my.cityu.edu.hk;

As climate change increases the frequency, intensity, and duration of heatwaves, understanding their impact on electricity grids is crucial for enhancing societal security and resilience. We study the effects of heatwaves on European electricity grids using several comprehensive real-world datasets. Moreover, noting that conventional modeling of temperature effects on grid operation limits is computationally challenging, we develop a novel temperature-dependent segment-based approach that is both efficient and accurate. We apply this method to evaluate the robustness of several European electricity grids for projected heatwave scenarios for the next 25 years. We find both concerning grid bottlenecks and national differences: for example, while the Spanish grid exhibits temperature-induced capacity bottlenecks that could jeopardize power supply during heatwaves, the German grid shows remarkable resilience. These findings emphasize the need for temperature-aware grid power flow analysis as well as the need for long-range planning to ensure energy security despite climate-change induced future heatwaves.

Introduction

Climate change has led to an increase in average global temperatures, characterized by more frequent, intense, and prolonged heatwaves [1–4]. The escalating frequency and severity of heatwaves impact millions of people worldwide [5] and pose significant challenges to critical infrastructure [6, 7] including electrical power grids [8]. A detailed understanding of these impacts on power grid performance is crucial for evaluating and enhancing societal resilience and energy security.

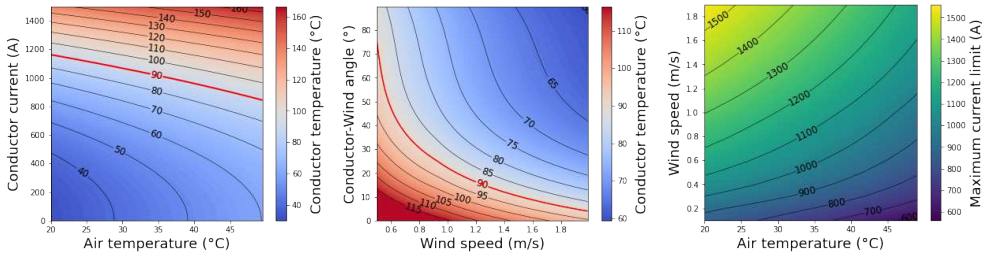
Heatwaves have a quadratic impact on electrical grids: not only increasing electrical cooling load but also reducing transmission line capacity due to reaching their thermal limits (see Fig. 1). Moreover, due to regional variations in air temperature, these thermally-induced capacity limits vary across different segments of a long-distance transmission, as shown in Fig. 2. Traditional power flow analyses do not accurately assess the impact of a heatwave for two reasons. First, existing linearized direct current (DC) power flow models, even if using a weather-dependent dynamic line rating, fail to capture complex interactions in grid dynamics under heavy cooling load, and thus cannot accurately evaluate thermal-induced grid vulnerability [9, 10]. Second, they typically fail to precisely model temperature effects on different segments of a single long transmission line. This oversight can lead to incomplete assessments of grid vulnerabilities, as our case studies for European electricity grids confirm [10, 11].

To address these two research gaps, we develop a novel temperature-aware, accurate, and efficient alternating current optimal power flow (ACOPF) analysis (Fig. 4). It incorporates three key innovations: (i) temperature-dependent cooling load estimation, (ii) using geospatially-gridded weather projections and (iii) per-segment conductor heat balance equations to determine thermal-dependent capacity limits for transmission lines, and an iterative temperature-dependent ACOPF (TD-ACOPF) analysis algorithm. We apply our approach to assess the effects of extreme weather on European electricity grids using the best publicly available weather projections, power demand, renewable penetration, and grid parameters. Our key findings and contributions are as follows:

▷ We demonstrate that existing grid resilience analysis based on standard ACOPF fails to adequately account for the combined effects of increased load demands and reduced current-carrying capacity during heatwaves. Even a state-of-the-art quadratic approximation to solve the TD-ACOPF problem [13] substantially underestimates the vulnerability of transmission lines.

▷ We develop a novel iterative TD-ACOPF algorithm incorporating both temperature-dependent cooling loads and thermally-induced capacity limits for each segment of a long transmission line, with weather effects modeled at a spatial resolution of approximately 30km × 30km. Our algorithm solves the TD-ACOPF problem efficiently and exactly.

▷ Using our approach, and based on the best available public data, our results for European electricity grids reveal significant cause for concern. By 2032, in certain scenarios, up to 6% of transmission lines are projected to reach the safety threshold of 70% of their current-carrying limits. There are also substantial national differences: the Spanish grid might suffer from significant load shedding, whilst the German grid demonstrates remarkable resilience. We caution that these results need to be further



(a) (b) (c)

Fig. 1: Physical properties of conductor form IEEE Std 738^{TM}-2012 under different weather conditions [12]. Fig. 1a shows conductor temperature under different air temperatures and line currents; Fig. 1b shows conductor temperature under different wind speeds and angles; Fig. 1c shows the maximum allowable current under different air temperatures and wind speeds.

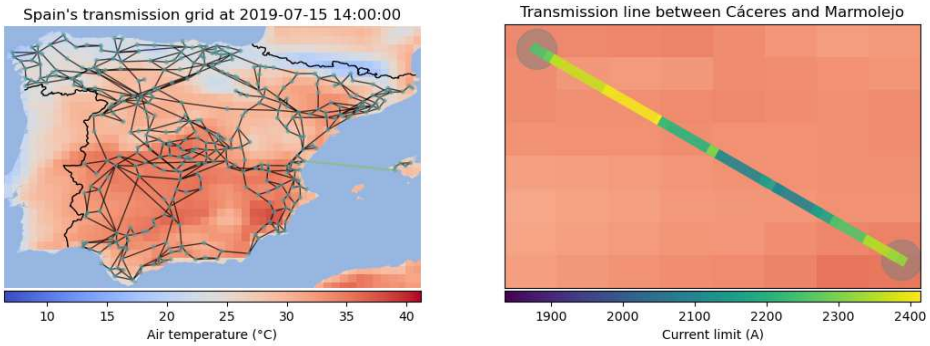


Fig. 2: Thermal-induced current-carrying capacities vary on different segments of long transmission lines in Spain. In this example, the long transmission line between Cáceres and Marmolejo is measured at 291 kilometers. It traverses across 15 geospatially-gridded regions, each with different air temperatures and wind speeds, resulting in different current-carrying capacities on different segments of the long transmission line.

validated using more detailed grid-specific data that is, unfortunately, not in the public domain.

These findings underscore the urgent need for grid operators and policymakers to consider the impacts of extreme weather more comprehensively in their planning and management strategies. By doing so, they can enhance the reliability and resilience of electricity supplies in the face of increasing climate change challenges.

Results

Setup

We employ the modeling framework described in Sec. 2 and the data sources outlined in Table 2 to evaluate how heatwaves impact grid operations in six European countries both for historical heatwave scenarios from 2019 and 2022 (focusing on the hottest hours of the year) and projected scenarios from 2025 to 2050. We conduct power flow analyses, investigating whether national grids exhibit temperature-induced capacity bottlenecks, indicated by the presence of load-shedding regions, that is, buses where the power injection fails to match consumption. Our work also compares the accuracy of existing power flow analysis methods with our new approach in identifying these critical bottlenecks whilst obeying physical constraints. Detailed simulation settings are provided in Sec. 3.

Figure 3 visually represents results for Spain through color-coded links and buses, depicting link current flows and load-shedding buses. Table 1 provides detailed statistics on grid status and load-shedding information. The evaluation metrics include (i) load-shedding ratio (unsatisfied demand to total demand) and affected regions; (ii) critical elements such as generators and branches exceeding 70% of their nameplate capacity and flow limits [14] and branches surpassing 70% of weather-dependent current limits [14]; (iii) average and maximum conductor temperatures are compared against the $90^{\circ}C$ safety rating [15–17]; (iv) normalized computational times for various power-flow analyses.

Complete simulation results for six countries are provided in Supplementary 1.

Observations

We find that, as heatwaves simultaneously reduce link capacity and increase cooling demand, some European national grids exhibit temperature-induced capacity bottlenecks leading to non-negligible load-shedding in projected heatwave scenarios. Unmet cooling demand during heatwaves can lead to potential human casualties [18–20]. These observations emphasize the need for temperature-aware grid analysis and planning to mitigate heatwave risks and ensure energy security.

In further detail, our analysis illustrates the limitations of conventional grid resilience analysis–based on the widely-used ACOPF approach–to accurately predict heatwave impacts on the electricity grid. This formulation does not model the thermal limits of links, leading to the presence of critical links with unsustainable high-current flows, as highlighted in Figure 3. More concretely, we note that in 2032, when air temperatures are projected to exceed $43^{\circ}C$, power flow analysis using standard ACOPF reveals only three load-shedding regions, underestimating the actual load shedding compared to the accurate temperature-dependent ACOPF (TD-ACOPF) analysis. Additionally, link temperatures are found to exceed the maximum allowable limit of $90^{\circ}C$ (reaching over $103^{\circ}C$) due to the neglect of line temperature constraints in the standard ACOPF analysis. This underscores the fact that standard ACOPF does not adequately capture the complex interactions between heat flow and power

Table 1: Results of grid resilience analysis for the 376-bus Spain's network under historical and projected heatwave scenarios. We observe that (i) Spain's grid exhibits temperature-induced capacity bottlenecks, and subsequently non-negligible load-shedding, in projected heatwave scenarios, resulting in non-negligible load-shedding. (ii) Existing grid resilience analyses, based on standard ACOPF and TD-ACOPF-quad, inaccurately capture the impact of heatwaves on transmission line capacity and underestimate the actual load-shedding. (iii) Our proposed approach, TD-ACOPF-iter, provides a precise representation closely aligned with the fully converged TD-ACOPF by effectively capturing these constraints through advanced heat-flow modeling while being computationally efficient.

Year	Air temp	Demand GW	Load-shedding ratio	Load-shedding region	Critical (above 70%) Gen.	Critical (above 70%) Line pow.	Critical (above 70%) Line cur.	Line temp. ave.	Line temp. max.	Norm. run-time
Model 0: ACOPF										
2019	29.3	36.0	0.0%	0	699	4	3	35.9	57.2	
2022	35.5	37.1	0.0%	0	661	17	13	43.3	74.3	
2028	37.0	44.7	0.2%	1	666	36	36	45.0	114.1	1.0
2032	43.9	50.1	1.2%	3	743	28	25	53.1	103.6	
2044	40.6	53.0	7.1%	22	729	20	11	49.0	81.9	
Model 1: TD-ACOPF-quad										
2019	29.3	36.0	0.0%	0	699	4	3	35.8	57.2	
2022	35.5	37.1	0.0%	0	660	17	15	43.3	92.9	
2028	37.0	44.7	0.2%	1	667	37	37	44.8	94.0	1.6
2032	43.9	50.1	1.7%	4	743	37	35	53.4	94.3	
2044	40.6	53.0	7.1%	23	729	21	12	48.9	81.5	
Model 2: TD-ACOPF-iter										
2019	29.3	36.0	0.0%	0	699	4	3	35.8	57.3	
2022	35.5	37.1	0.0%	0	654	20	14	43.4	90.0	
2028	37.0	44.7	0.2%	1	668	37	38	44.8	90.0	2.2
2032	43.9	50.1	1.8%	5	743	37	35	53.4	90.0	
2044	40.6	53.0	7.1%	23	729	21	12	48.9	81.5	
Model 3: TD-ACOPF										
2019	29.3	36.0	0.0%	0	699	4	3	35.8	57.3	
2022	35.5	37.1	0.0%	0	655	20	15	43.4	90.0	
2028	37.0	44.7	0.2%	1	672	39	39	44.9	90.0	7.6
2032	43.9	50.1	1.8%	5	743	38	37	53.4	90.0	
2044	40.6	53.0	7.1%	23	729	21	12	48.9	81.5	

flow under extreme heatwave conditions, resulting in inaccurate grid status estimations. Such inaccuracies could potentially lead to link shutdown or even grid blackout if the power generation plan derived from the ACOPF analysis is executed during heatwaves [18–20].

In contrast, the TD-ACOPF formulation offers a more precise representation by effectively capturing these constraints through advanced heat flow modeling [21], ensuring reliable assessment of grid performance under stress, albeit at a higher computational cost. To address this cost, our proposed TD-ACOPF-iter (iterative TD-ACOPF analysis) incurs lower computational cost yet aligns closely with the TD-ACOPF results. As seen in Table 1, our iterative analysis requires only about twice the computational cost of solving standard ACOPF, while the fully converged TD-ACOPF

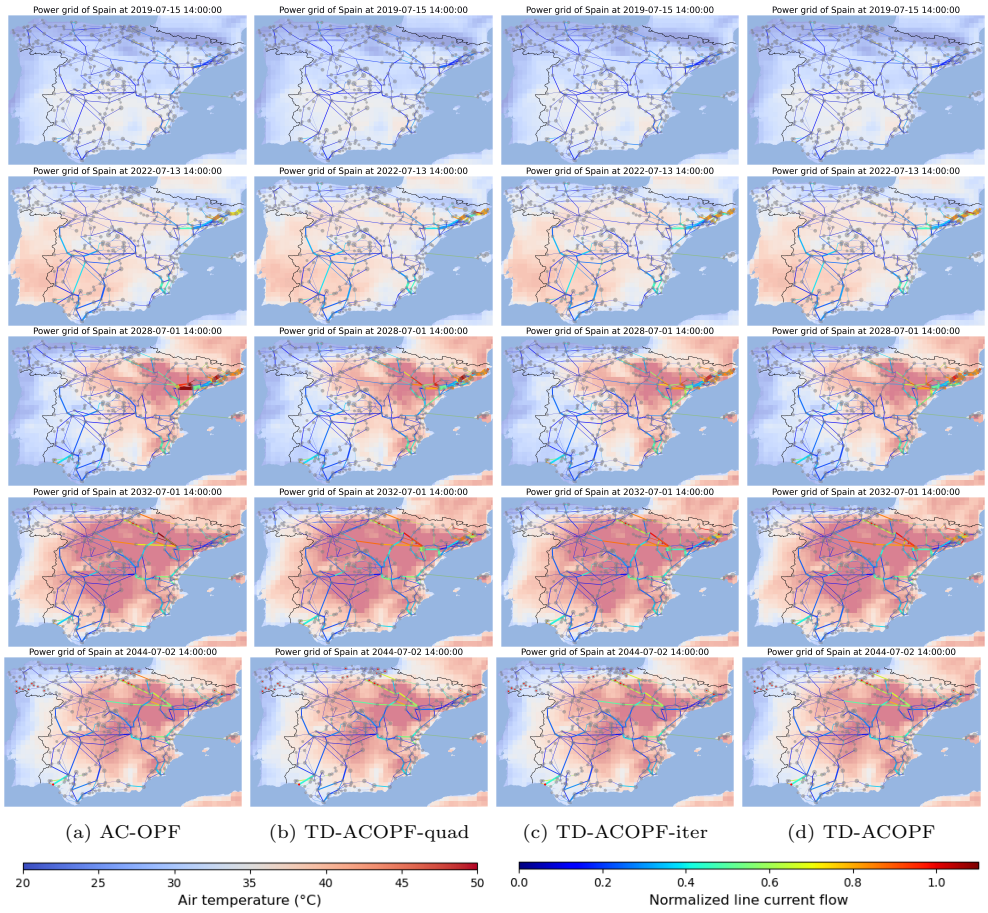


Fig. 3: Color-coded link current flows and load-shedding regions (red circle) from power-flow analysis of the transmission network in Spain under historical and projected heatwave scenarios. The figures progress from left to right columns, depicting results of ACOPF, TD-ACOPF-quad, TD-ACOPF-iter, and TD-ACOPF, respectively. Together with Table 1, the results show that (i) Spain's grid exhibits temperature-induced capacity bottlenecks in projected heatwave scenarios, resulting in non-negligible load-shedding, and (ii) the load-shedding ratios and regions can be accurately and efficiently computed by our proposed TD-ACOPF-iter method.

incurs more than seven times the cost. This enhancement significantly facilitates faster and more reliable grid resilience analysis, crucial for real-time decision-making during climatic emergencies.

We further find that other state-of-the-art alternatives, i.e., those based on standard ACOPF and TD-ACOPF-quad (using a quadratic approximation of the temperature-dependent current-carrying limit constraints), underestimate the load-shedding regions. For 2032 again, for example, TD-ACOPF-quad only estimates 4

load-shedding regions, instead of 5 identified by the TD-ACOPF analysis and our iterative analysis, as illustrated in Fig. 3 and quantified in Table 1. Furthermore, in 2022, 2028, and 2032, analyses using the TD-ACOPF-quad with the quadratic approximation of heat flow violate the temperature constraints of conductors. This demonstrates that our approach assesses grid status more accurately than previous studies, making it a suitable method for power flow analysis under extreme heatwaves.

Last but not least, our findings highlight significant national differences in grid robustness across Europe. Detailed analyses for six countries (Supplementary 1) reveal that Spain's electricity grid is susceptible to critical bottlenecks that could jeopardize power supply during heatwaves with potential severe societal consequence [18], while Germany's infrastructure shows substantial resilience. Stress tests for European grids in 2025 (Supplementary 2) further underscore these differences: Germany's grid continues to function under increased thermal stress, whereas Spain's network exhibits capacity bottlenecks at a critical threshold of $33°C$. This divergence emphasizes the need for tailored, region-specific strategies in grid management and infrastructure development to mitigate the adverse effects of extreme weather conditions.

Limitations

Whilst concerning, we note that our results are based on publicly-available models for European grids, which do not have the granular detail available to grid operators themselves. Moreover, although we use the currently best-available locally bias-corrected weather projections [22–24], these projections themselves are subject to revision as forecasting technology and climate models improve.

Broader Implication

Our insights suggest that grid operators periodically re-evaluate grid resilience assessments and planning using the methodologies presented in this work, along with their own granular grid model and the latest climate projections. This would allow them and policymakers to assess their preparedness for climate-induced disruptions, ensuring a more secure and reliable energy supply in the face of increasingly frequent and severe weather events.

Discussion and Conclusion

Despite the urgent need to assess the potential impact of extreme heat events on the electrical transmission grid, existing approaches neither account for their simultaneously increasing demand and decreasing transmission line power-carrying capacity nor are computationally efficient. Moreover, existing models ignore the locally weather-dependent AC power flow limit of each segment of a transmission line. To address these research gaps, we present segmented and computationally efficient power flow modeling of a long transmission line. We combine this with a geospatially-gridded weather forecast to assess the resilience of different European national grids to extreme weather events. We further propose an efficient iterative algorithm to solve the problem with high accuracy and without making approximations, as compared with previous studies.

As a result, we find that there is a significant variation in resilience, with Germany's grid well able to cope with extreme weather with capacity to spare, unlike Spain's grid.

The heatwave-induced capacity bottlenecks and potential load shedding identified by our work can be mitigated using one of the three following approaches. First, load shedding or demand response on the load centres served by such links can maintain grid integrity albeit at the cost of inconveniencing many consumers. Second, reconductoring existing transmission lines increases their capacity and resilience but requires capital investment and a significant lead time. Our work identifies the specific transmission lines that need such re-conducting. A third approach would be to place storage at each end of a bottleneck transmission line, so that storage discharge can be used to compensate for transmission limits. With the advent of grid-scale storage, such an approach might become economically feasible and is a topic we intend to investigate in our future work.

Our results rely on diverse datasets not all of which are easy to obtain. To make our work replicable and to aid the research community, our collated dataset will be openly shared, along with our algorithms and source code.

Our work suffers from some key limitations. First, although we rely on the best-available data sets for grid topology, weather reanalysis, and long-range weather forecasts, we assume that our data sources are error-free. Errors in underlying data will naturally affect our conclusions. We recommend that grid operators use their private and more granular grid topology models along with our methodology to assess grid resilience to heatwaves. Second, our iterative analysis approach has been validated only with respect to the TD-ACOPF model, rather than ground truth. Finally, our work only addresses capacity problems, but not the relative costs and benefits of different mitigation solutions. We hope to address these limitations in future work.

Methods

1 Data Sources

We summarize the real-world publicly-available datasets used in our study in Table 2, encompassing the European transmission grid, historical and future projected weather data, power demand profiles, and renewable generation models.

Table 2: Summary of data sources.

Data	Description
PyPSA-Eur [14]	Open-source dataset of European transmission network
ERA5 [25]	Historical hourly global climate data from ECMWF reanalysis
C3S [23, 24]	Future reference climate data from C3S Energy operational service
ENTSO-E [26]	Historical hourly country-level power demand data
Demand.ninja [27]	Future weather-dependent energy demand models
Atlite [28]	Open-source model for renewable generation calculation

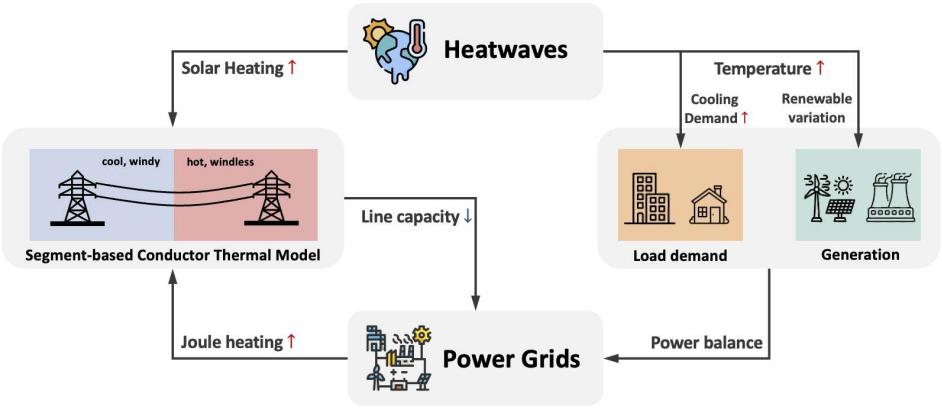


Fig. 4: The proposed framework combines segment-weather-dependent conductor thermal modeling, temperature-dependent demand modeling, weather-dependent renewable generation, future heatwave modeling, and power flow modeling to reveal temperature-induced capacity bottlenecks in European power grids during heatwaves.

2 Model and Algorithm

We develop a novel power flow analysis framework to accurately and efficiently assess the resilience of the European power grid under extreme heatwaves. As depicted in Fig. 4, this framework integrates several key components as follows:

- Future Heatwave Projection (Sec. 2.1): it generates projected heatwave events from 2025 to 2050 based on historical heatwaves from 2019 and 2022.
- Future Demand Modeling (Sec. 2.2): it utilizes Demand.ninja [27] to model power demand considering the weather condition and annual growth.
- Renewable Generation: it leverages existing frameworks from Atlite [28] to calculate renewable generation given weather conditions.
- Conductor Thermal Modeling (Sec. 2.3): it analyzes the impact of elevated temperatures on conductor physical properties and their effects on thermal limits.
- Multi-Segment Modeling (Sec. 2.4): it models the transmission line at segmented levels to identify localized stress points and potential bottlenecks.
- Optimal Power Flow Analysis (Sec. 2.5): it integrates these components to simulate the grid's response under thermal and demand stresses, revealing potential capacity bottlenecks and load shedding regions.

2.1 Future Heatwave Modeling

We adopt the future reference climate variables with bias correction based on the European regional climate model, CORDEX, under the RCP 4.5 scenario for the European domain [29]. However, these reference climate data are averaged over three hours and do not adequately capture shorter-duration extreme heat events. To address

this issue, we apply the following "morphing" approach to artificially create heat events [30]. The process is as follows:

- We first select temperature profiles from historical heatwave events in the ERA5 dataset, denoted as $T^{\text{his}}_{\text{heat}}$, and the historical reference temperature data, $T^{\text{his}}_{\text{ref}}$, in the same historical date.
- To derive the projected future heatwave scenarios $T^{\text{fut}}_{\text{heat}}$ from the future reference temperature $T^{\text{fut}}_{\text{ref}}$, we calculate it as $T^{\text{fut}}_{\text{heat}} = T^{\text{fut}}_{\text{ref}} + (T^{\text{his}}_{\text{heat}} - T^{\text{his}}_{\text{ref}})$.

As shown in Supplementary Fig. 1, the projected future heatwave exhibits a similar increase relative to the reference temperature when compared to a historical heatwave event. This "morphing" approach offers a simple yet effective method for simulating future extreme events, thereby facilitating the study of power grid resilience under such conditions.

2.2 Future Demand Modeling

We employ the Demand.ninja [27] to model the future daily demand as follows:

$$P_{\text{total}} = P_{\text{base}} + P_{\text{heat}}[T_{\text{heat}} - \text{BAIT}]^{+} + P_{\text{cool}}[\text{BAIT} - T_{\text{cool}}]^{+} + \alpha W + \beta D + \epsilon \quad (1)$$

where P_{base} is in GW, P_{heat} and P_{cool} are $GW/^{\circ}C$ and ϵ is the model error term. α (in GW) and β (in GW/yr) are time coefficients, representing the impacts of differences in weekdays and long-term trends in power demand. T_{heat} and T_{cool} are the heating and cooling threshold. BAIT denotes the building-adjusted internal temperature derived from [27] and depends on specific weather conditions such as air temperature, wind speed, and solar radiation. The calibrated model for six countries, reflecting the historical demand profile, is illustrated in Supplementary Fig. 2. This model incorporates the cooling threshold and cooling coefficient, which account for the impact of heatwaves on power demand. For future electricity demand from 2025 to 2050, we use an annual growth rate of 1.1% [31]

After generating daily power demand, we convert it to an hourly resolution based on the historical average hourly demand ratios observed during hot days, following [27]. This hourly demand profile is considered a conservative estimation, as it does not fully account for the increasing cooling demand during the hottest hours.

2.3 Conductor Thermal Modeling

The steady-state heat balance equation is used to determine the thermal behavior of overhead conductors under steady-state conditions. It accounts for the balance between the heat generated in the conductor due to electrical current (I^2R losses) and the heat lost to the surroundings through convection, radiation, and conduction. It provides a comprehensive method for calculating the temperature of the conductor, ensuring safe and efficient operation within its thermal limits. The equation considers various factors, including ambient temperature, wind speed, solar radiation, and conductor properties.

The specific steady-state heat balance equation according to IEEE Std 738$^{\text{TM}}$-2012 [12] used in our study is as follows:

$$\underbrace{H_C + H_R}_{\text{heat loss}} = \underbrace{H_S + H_J}_{\text{heat gain}} \quad [\text{W/m}], \tag{2}$$

where

$$H_C = \max \begin{cases} 3.645\rho_f^{0.5} D^{0.75} \left(T_c - T_a\right)^{1.25}, & \text{(zero wind speed)}; \\ K_\phi \left[1.01 + 1.35 N_{\text{Re}}^{0.52}\right] \lambda_f \left(T_c - T_a\right), & \text{(low wind speed)}; \\ 0.754 K_\phi N_{\text{Re}}^{0.6} \lambda_f \left(T_c - T_a\right), & \text{(high wind speed)}; \end{cases} \tag{3}$$

$$H_R = \pi \sigma_B D \alpha_{\text{emi}} \left[\left(T_c + 273\right)^4 - \left(T_a + 273\right)^4\right] \tag{4}$$

$$H_S = \alpha_{\text{abs}} D S \tag{5}$$

$$H_J = I^2 R(T_c) = I^2 R_{\text{ref}}(1 + \alpha_r(T_c - T_{\text{ref}})) \tag{6}$$

Here H_C is the heat loss rate due to convective cooling affected by air temperature, wind speeds, angles, and the conductor temperature; H_R is the heat loss rate due to radiative cooling caused by the temperature difference, H_S is the heat gain rate due to solar radiation and H_J is the heat gain rate due to Joule heating under conductor current and temperature-dependent resistance. The values of these coefficients are specified in Table 3.

Table 3: Parameters in the conductor thermal model.

Notation	Description
ϕ	The angle between wind and axis of conductor, taking value in $[0, \pi/2]$
K_ϕ	Wind direction factor, $K_\phi = 1.194 - \cos(\phi) + 0.194\cos(2\phi) + 0.368\sin(2\phi)$
V_{w}	Wind speed [m/s]
D	Conductor diameter [m]
L	Conductor length [m]
S	Total solar heat intensity [W/m^2]
N_{re}	Dimensionless Reynolds number, $N_{\text{re}} = D\rho_f V_{\text{w}}/\mu_f$
ρ_f	Density of air [kg/m^3]
μ_f	Dynamic viscosity of air
λ_f	Thermal conductivity of air [W/(m $\cdot$ °C)]
α_{emi}	Radiation emissivity factor, taking values in $[0, 1]$
α_{abs}	Solar absorptivity factor, taking values in $[0, 1]$
α_r	Temperature-dependent resistance coefficient
σ_B	Stefan–Boltzmann constant $\sigma_B = 5.67 \times 10^{-8}$ [W/(m$^2 \cdot$ K^4)]
T_c, T_a, T_r	Conductor, air, and reference temperature [°C]
$R(T_c)$	Unit temperature-dependent resistance [Ω/m]

To illustrate the heat balance under varying meteorological conditions, we conducted simulations using the steady-state temperature model with default parameters derived from the 795 kcmil 26/7 Drake ACSR conductor. The heat balance equation,

a single-variable nonlinear equation, is efficiently solved using Newton's method. The simulation results are presented in Fig. 1, leading to several important observations:

- As shown in Fig. 1a, the steady-state temperature of the conductor rises monotonically with an increase in either the conductor current, which induces Joule heating, or the air temperature.
- Fig. 1b illustrates that the steady-state temperature of the conductor decreases as the wind speed or the wind-conductor angle increases, both of which enhance convective heat loss.
- In Fig. 1c, it demonstrates that under specific weather conditions, given the maximum allowable temperature of the conductor as 90 $^{\circ}C$, the maximum permissible current can be uniquely determined. Hence, the transmission line temperature constraint can be equivalently converted as the line current constraint, simplifying the power flow analysis [32].

2.4 Multi-segment Modeling

To capture the impact of spatially heterogeneous weather for long-distance links, we compute the intersection of the line with the grid lines implicitly embedded in gridded weather datasets such as ERA5 (see Fig. 2) [10]. Segments within a single grid cell share the power flow and current, but have different resistances due to thermal effects under various local weather conditions, such as wind speed and solar radiation. For each link, the multi-segment model satisfies the following equations:

$$H_{C,l,s} + H_{R,l,s} = H_{S,l,s} + I_l^2 R(T_{l,s}),\ \forall s \in \mathcal{S}_l \tag{7}$$

$$T_{l,s} \leq T^{\max},\ \forall s \in \mathcal{S}_l \tag{8}$$

$$R_l = \sum_{s \in \mathcal{S}_l} d_{l,s} \cdot R(T_{l,s}), \tag{9}$$

where conductor temperature for each segment $s \in \mathcal{S}_l$ from line l in Equation (7) is derived from the heat balance equation from Equations (2) to (6) at each line segment under local weather conditions. We also enforce the constraint that the segment temperature is upper bounded in Equation (8). The total transmission line resistance is equal to the summation of segment resistance in Equation (9). This results in the branch flow being constrained by the segment that has the highest temperature. Note that our approach is compatible with any gridded weather dataset, so that as these data products become more fine-grained over time, our segmented transmission line model automatically becomes more accurate.

2.5 Optimal Power Flow Analysis

The Optimal Power Flow (OPF) problem is a fundamental component in electricity grid operations and vulnerability analysis. It aims to determine the most efficient operating conditions for an electrical power system, ensuring that power generation meets the demand while minimizing operational costs and adhering to system constraints. In the context of grid vulnerability analysis, it can be used to identify weak points and

assess the robustness and resilience of the grid to potential disruptions, including the heatwaves studied in this paper, as well as enhance its reliability and stability under various stress conditions.

We first introduce the standard Alternating-current OPF (ACOPF) problem in Sec. 2.5.1 and extend to include conductor thermal modeling within the Temperature-dependent ACOPF (TD-ACOPF) in Sec. 2.5.2. The proposed iterative algorithm for solving TD-ACOPF is in Sec. 2.6.

2.5.1 Alternating-current OPF (ACOPF)

To our knowledge, the most standard OPF formulation based on the Alternating Current (AC) model is AC Optimal Power Flow (ACOPF) [33]. It is a non-linear, constrained optimization problem that incorporates both the physical laws governing power flow and the operational limits of the grid components: for a grid with parameters shown in Table 4,

$$\min \quad \sum_{i\in\mathcal{N}} \sum_{k\in\mathcal{G}_i} c_{i,k} \cdot P_{g,i,k}, \tag{10}$$

$$\text{s.t.} \quad \sum_{k\in\mathcal{G}_i} P_{g,i,k} - P_{d,i} = \text{re}\left(V_i (\sum_{j\in\mathcal{N}} Y_{ij} V_j)^* \right), \ \forall i \in \mathcal{N}, \tag{11}$$

$$\sum_{k\in\mathcal{G}_i} Q_{g,i,k} - Q_{d,i} = \text{im}\left(V_i (\sum_{j\in\mathcal{N}} Y_{ij} V_j)^* \right), \ \forall i \in \mathcal{N}, \tag{12}$$

$$P_{g,i,k} \in [P^{\min}_{g,i,k}, \ P^{\max}_{g,i,k}], \ Q_{g,i,k} \in [Q^{\min}_{g,i,k}, Q^{\max}_{g,i,k}], \ \forall i \in \mathcal{N}, \ \forall k \in \mathcal{G}_i, \tag{13}$$

$$|V_i| \in [V_m^{\min}, V_m^{\max}], \ \forall i \in \mathcal{N}, \tag{14}$$

$$|\angle V_i - \angle V_j| \leq V_a^{\max}, \ \forall l = (i,j) \in \mathcal{L}, \tag{15}$$

$$|V_i \left((V_i - V_j) \, Y_{ij} \right)^* | \leq S_{ij}^{\max}, \ \forall l = (i,j) \in \mathcal{L}, \tag{16}$$

$$Y_l = 1/(R_l + \mathrm{i} \cdot X_l), \ \forall l = (i,j) \in \mathcal{L}, \tag{17}$$

$$\text{var. } \boldsymbol{P}, \boldsymbol{Q}, \text{ and } \boldsymbol{V}.$$

The objective function in (10) represents the total generation cost, approximated as a linear function of active generations from individual generators. The non-linear power flow balance constraints in (11)-(12) ensure that the injection and load are balanced at every single bus. The generation, voltage, and line flow constraints are in (13)-(16).

2.5.2 Temperature-dependent ACOPF (TD-ACOPF)

The Temperature-Dependent AC Optimal Power Flow (TD-ACOPF) problem extends the standard ACOPF formulation by incorporating the impact of weather on the electrical network's parameters [9, 11, 34]. This includes adjusting line resistances and current-carrying capacities based on temperature, which affects the power flow and operational constraints. The particular TD-ACOPF formulation considered in this

Table 4: Parameters of the power grid model.

Notation	Description
$\mathcal{N}$	set of buses
$\mathcal{L}$	set of lines
$\mathcal{G}_i,\ \forall i \in \mathcal{N}$	set of generators at each bus
$\mathcal{S}_l,\ \forall l \in \mathcal{L}$	set of segments at each line
$V_i,\ \forall i \in \mathcal{N}$	complex voltage at each bus
$P_{d,i}, Q_{d,i},\ \forall i \in \mathcal{N}$	active and reactive power demand at each bus
$P_{g,i,k}, Q_{g,i,k},\ \forall i \in \mathcal{N},\ \forall k \in \mathcal{N}_i$	active and reactive power generation for each generator
$c_{i,k},\ \forall i \in \mathcal{N},\ \forall k \in \mathcal{N}_i$	generation cost for each generator
$P_l, Q_l, I_l,\ \forall l = (i,j) \in \mathcal{L}$	active, reactive power flow and current at each line
$T_{l,s},\ \forall l \in \mathcal{L},\ \forall s \in \mathcal{S}_l$	temperature for each segment at each line
$d_{l,s},\ \forall l \in \mathcal{L},\ \forall s \in \mathcal{S}_l$	length for each segment at each line
Y, G, B, R, X	admittance, conductance, susceptance, resistance, reactance

paper is given as follows:

$$\begin{aligned} \min\quad & (10) \\ \text{s.t.}\quad & (11)-(17) \\ & I_l = |(V_i - V_j)Y_{ij}|,\ \forall l = (i,j) \in \mathcal{L}, \\ & (2)-(9),\ \forall l = (i,j) \in \mathcal{L} \\ \text{var.}\quad & \boldsymbol{P}, \boldsymbol{Q},\ \text{and}\ \boldsymbol{V}. \end{aligned} \tag{18}$$

In this formulation, the standard ACOPF constraints specified from (11) to (17) determine the line current magnitude as described in (18). This current leads to Joule heating, which subsequently increases conductor temperatures. Additionally, the constraints from (2) to (9) model heat transfer in individual transmission line segments under varying weather conditions. These constraints ensure the maintenance of permissible steady-state conductor temperatures, influencing the line current-carrying capacities. The interdependence of electrical and thermal constraints in the TD-ACOPF model presents challenges in determining the optimal power generation scheme.

2.6 Algorithm Design

For standard ACOPF, Interior Point Methods (IPMs) have demonstrated effectiveness across various IEEE test scenarios [35, 36]. Extending these methods to solve TD-ACOPF markedly increases complexity due to the interdependence of electrical and thermal constraints, as summarized in Table 5.

2.6.1 Existing Methods for Solving TD-ACOPF

Existing studies adopt different approximation methods to solve TD-ACOPF.

- Linear approximation (DC-OPF and TD-DCOPF): This approach linearizes the nonlinear constraints in ACOPF and incorporates weather-dependent dynamic line ratings [10, 11, 37]. However, it generally overlooks the interactions between heat

Table 5: Summary of approaches for power flow analysis under heatwaves.

Methods	Power Flow	Heat Flow	Multi-Segment	Accuracy	Complexity
DCOPF	Linear	✗	✗	Low	Low
ACOPF	Non-linear	✗	✗	Low	Medium
TD-DCOPF	Linear	dynamic line rating	✓	Low	Low
TD-ACOPF	Non-linear	Non-linear	✓	High	High
TD-ACOPF-quad.	Non-linear	quadratic heat flow	✓	Medium	Medium
TD-ACOPF-iter.	Non-linear	Non-linear	✓	High	Medium

flow and power flow, potentially leading to substantial inaccuracies in the resolved power flows.

- Quadratic approximation (TD-ACOPF-quad): Some models use a quadratic function to estimate steady-state conductor temperature [13], expressed as $T_c \approx \beta_0 + \beta_1 I^2 + \beta_2 I^4$ with weather-dependent coefficients $\{\beta_0, \beta_1, \beta_2\}$. This simplified version of the heat balance equation is then integrated into the standard ACOPF model.

While these approximations enhance computational efficiency, they frequently fail to fully meet the rigorous demands of the heat and power balance equations, particularly under the stringent conditions imposed by temperature constraints. Often, these methods overlook potential capacity constraints, which can result in inaccuracies when evaluating grid performance under extreme weather scenarios.

Despite these advancements, the development of an efficient algorithm capable of solving the exact version of TD-ACOPF with multi-segment modeling has been a significant gap in the field that we address in this work.

2.6.2 Proposed iterative algorithm (TD-ACOPF-iter)

Algorithm 1 Iterative optimization for TD-ACOPF

Data: Weather data, conductor thermal model, and power gird model.
Result: Grid operational state under OPF analysis.

For each segment, given the gridded weather data, transform the temperature limit to the current constraint as Equation (19).
For each line, select the minimum current limit among segments as the line current constraint.
while *conductor temperature not converge* **do**
    Update temperature-dependent admittance for each segment of each line.
    Aggregate segment admittance into line admittance for ACOPF model.
    Solve the standard ACOPF with additional line current constraints by IPM.
    Update the line current derived from the OPF analysis.
    Solve the heat flow equation of all segments using Newton's methods.
    Update the segment temperature derived from heat flow equations.
end

To efficiently solve TD-ACOPF, we have developed an innovative iterative algorithm, detailed in Algorithm 1. This algorithm is designed around two key steps that improve computation efficiency and improve solution accuracy:

- We convert the steady-state conductor temperature constraints into equivalent conductor current constraints based on weather conditions of local segments [10, 37]. This transformation, represented by Equation (19), eliminates the need for explicit steady-state temperature expressions, effectively decoupling the heat and power balance equations. This strategy simplifies the model while ensuring the safety of lines under temperature constraints:

$$I^{\max} = \sqrt{(H_C + H_R - H_S)/(R(T^{\max}))}, \tag{19}$$

  where the heat gain and loss are calculated under the maximum allowable temperature.
- Motivated by the decoupling approach for solving TD power flow equations in [9, 38], we develop an alternating updating mechanism where (i) the ACOPF is solved with the additional current constraints derived from (19) and (ii) the heat balance calculation is conducted independently for each segment. Empirical evaluations suggest that, typically, only two iterations of this process are required to achieve results nearly as precise as those from fully converged solutions.

By decoupling heat and power balance constraints, the algorithm provides flexibility and precision for accessing grid status characterized by varied thermal and electrical properties. Thus, the proposed algorithm not only fills a significant research gap in the OPF study by providing an efficient solution for TD-ACOPF but also enhances the ability of precise power grid analysis for policy-making under extreme weather conditions. This development marks a substantial advancement in grid management technologies, offering utilities the tools to better predict and mitigate the impacts of thermal stress on power distribution systems. This is increasingly crucial in an era where climate variability introduces new challenges to maintaining stable and reliable energy supplies.

3 Application to the European Electricity Grid

To investigate the resilience of the European electricity grid under historical and projected future heatwaves, we integrate the data sources outlined in Table 2 and utilize the modeling framework described in Section 2. Simulations were conducted for six European countries, with detailed settings provided in Table 6. Key aspects of these simulations include:

- We selected six countries that were significantly impacted by the heatwave in July 2019.
- Utilizing the PyPSA-Eur framework, we model the power grid for European countries shown in Table 7. The configurations for the power grid include:
  - **Network resolution**: To mitigate local modeling inaccuracies, such as misassignment of load and supply and under-representation of inner-city underground

Table 6: Simulation settings for the European electricity grid.

Settings	Descriptions
Simulated countries	Belgium, Italy, Spain, Germany, France, and the UK.
Simulated period	historical heatwave in 2019 and 2022, future heatwaves from 2025-2050.
Basic Grid model	PyPSA-Eur derived realistic transmission network [14].
Compared algorithm	ACOPF, TD-ACOPF-quad, TD-ACOPF-iter, TD-ACOPF.

Table 7: Configurations of European Power grid derived from PyPSA-Eur.

Country	Buses	Lines	Generators		Installed Capacity (GW)	
			Conventional	Renewable	Conventional	Renewable
Belgium	39	47	24	64	12.33	10.34
France	417	660	271	852	69.47	29.10
Italy	235	368	83	476	56.49	32.43
Spain	376	624	84	721	39.96	38.87
Germany	339	486	415	528	79.21	115.96
UK	226	323	239	529	54.22	37.95

cabling, we adopt a clustered grid network. This approach merges nearby buses and lines to simplify the grid representation, reducing potential error-induced bottlenecks [14]. We determine the aggregation level for each country to ensure there were no infeasibilities during historical heatwave conditions, thus aligning with known real-world outcomes.

- **Line connection**: All under-construction lines were included during network creation, enhancing grid connectivity and providing a more optimistic assessment of grid capacity under stress conditions [14].
- **Line type**: We standardized the transmission lines to "Al/St 240/40 4-bundle 380.0", with an Aluminium/Steel cross-section of 240/40 and a 4-bundle configuration of wires per phase at 380 kV [14, 39].
- **Line capacity**: Unlike PyPSA-Eur's default setting of 70% maximum branch flow, our model permits 100% utilization, offering a optimistic assessment of grid capacity under stress conditions.
- **Thermal limits**: The traditional Aluminum/Steel conductors (e.g., ACSR, AAC, AAAC) typically operate between 80°C and 120°C [15–17, 40]. We also noted that a few high-temperature low sag conductors (HTLS) have been installed for field testing in Europe [41], capable of withstanding temperatures up to 210°C. In our simulations, we consider a typical maximum operating temperature of 90°C for Aluminum-type conductors [13, 42].

- In adapting the PyPSA-Eur data, primarily suited for DC/economic dispatch models, for our TD-ACOPF simulations, we recognize the necessity to include several critical elements not originally detailed. Our assumptions are as follows:
  - **Voltage bounds**: We adhere to typical grid standards by setting the voltage magnitude within a specified operational range, $0.95 \leq V_m \leq 1.05$ [36].

- **Reactive Load Demand**: Echoing recommendations from EnerPol [43], we assume that the reactive power demand (Q_d) is proportionally related to the active power demand. Specifically, $Q_d = 0.15 \cdot P_d$. This assumption simplifies the modeling of reactive power needs by directly linking it to active power, reflecting typical consumption patterns.
- **Other AC-OPF constraint**: We relax other AC-OPF related constraints [10], such as reactive generation capacity and branch phase angle constraints. By doing so, we aim to provide an optimistic yet plausible assessment of the grid's capacity under stress conditions.

In summary, our model adopts a conservative approach in several key aspects: it features an aggregated and more interconnected network topology, permits 100% utilization of branches, and relaxes some constraints. This strategy enables us to explore the upper limits of grid performance, allowing for the identification of potential bottlenecks and stress points. These insights are crucial for pinpointing areas that may require more stringent controls under actual operating conditions. Furthermore, we recognize the need for further tightening of these constraints with more realistic data to ensure a more accurate and realistic evaluation of grid capabilities.

Author contributions

S.K. and M.C. conceived the study. E.L. collected the data for motivation and experiments. E.L., M.C., and S.K. developed the formulation. E.L. developed the algorithm. E.L. conducted the experiments. E.L., M.C., and S.K. analyzed the algorithm performance and experimental results. E.L., M.C., and S.K. wrote and improved the manuscript.

Data availability

The results from the model that support the findings of this study are presented in the main text and Supplementary Information. The data used for validation are publicly available from the sources listed in Table 2.

Code availability

The TD-ACOPF-iter algorithm developed in this study is available in the GitHub repository (https://github.com/emliang/Heatwave.Impact.on.EU.Grid). The code is implemented in Python and can be accessed for replication and further research.

References

[1] IPCC. *Climate Change 2021: The Physical Science Basis. Contribution of Working Group I to the Sixth Assessment Report of the Intergovernmental Panel on Climate Change* (Cambridge University Press, Cambridge, United Kingdom and New York, NY, USA, 2021).

[2] Perkins-Kirkpatrick, S. & Lewis, S. Increasing trends in regional heatwaves. *Nature Communications* **11**, 3357 (2020).

[3] Miranda, N. D. *et al.* Change in cooling degree days with global mean temperature rise increasing from 1.5 c to 2.0 c. *Nature Sustainability* **6**, 1326–1330 (2023).

[4] Vautard, R. *et al.* Heat extremes in western europe increasing faster than simulated due to atmospheric circulation trends. *Nature Communications* **14**, 6803 (2023).

[5] Ballester, J. *et al.* Heat-related mortality in Europe during the summer of 2022. *Nature Medicine* **29**, 1–10 (2023).

[6] Liu, L. *et al.* Climate change impacts on planned supply–demand match in global wind and solar energy systems. *Nature Energy* 1–11 (2023).

[7] Sun, Y. *et al.* Global supply chains amplify economic costs of future extreme heat risk. *Nature* **627**, 797–804 (2024).

[8] Xu, L. *et al.* Resilience of renewable power systems under climate risks. *Nature Reviews Electrical Engineering* **1**, 53–66 (2024).

[9] Frank, S., Sexauer, J. & Mohagheghi, S. Temperature-dependent power flow. *IEEE Transactions on Power Systems* **28**, 4007–4018 (2013).

[10] Glaum, P. & Hofmann, F. Leveraging the existing german transmission grid with dynamic line rating. *Applied Energy* **343**, 121199 (2023).

[11] Neumann, F., Hagenmeyer, V. & Brown, T. Assessments of linear power flow and transmission loss approximations in coordinated capacity expansion problems. *Applied Energy* **314**, 118859 (2022).

[12] Ieee standard for calculating the current-temperature relationship of bare overhead conductors. *IEEE Std 738-2012 (Revision of IEEE Std 738-2006 - Incorporates IEEE Std 738-2012 Cor 1-2013)* 1–72 (2013).

[13] Ngoko, B. O., Sugihara, H. & Funaki, T. Optimal power flow considering line-conductor temperature limits under high penetration of intermittent renewable energy sources. *International Journal of Electrical Power & Energy Systems* **101**, 255–267 (2018).

[14] Hörsch, J., Hofmann, F., Schlachtberger, D. & Brown, T. Pypsa-eur: An open optimisation model of the european transmission system. *Energy strategy reviews* **22**, 207–215 (2018).

[15] Nigol, O. & Barrett, J. Characteristics of acsr conductors at high temperatures and stresses. *IEEE Transactions on Power Apparatus and Systems* 485–493 (1981).

[16] Douglass, D. & Reding, J. Ieee standard for calculating the current-temperature of bare overhead conductors. *IEEE Standard* 738–2006 (2007).

[17] Abboud, A. W., Gentle, J. P., Parikh, K. & Coffey, J. Sensitivity effects of high temperature overhead conductors to line rating variables. Tech. Rep., Idaho National Lab.(INL), Idaho Falls, ID (United States) (2020).

[18] Naumann, G. *et al.* Global warming and human impacts of heat and cold extremes in the eu. *Crop Pasture Sci* **10**, 47878 (2020).

[19] Stone Jr, B. *et al.* How blackouts during heat waves amplify mortality and morbidity risk. *Environmental Science & Technology* **57**, 8245–8255 (2023).

[20] Calli, M. E. Climate and capacity: Why power outages are surging around the world. https://www.aa.com.tr/en/environment/climate-and-capacity-why-power-outages-are-surging-around-the-world/3262691 (2024). Accessed: 2024-09-10.

[21] Kanálik, M., Margitová, A., Urbanskỳ, J. & Beňa, L. *Temperature calculation of overhead power line conductors according to the cigre technical brochure 207*, 1–5 (IEEE, 2019).

[22] Copernicus Climate Change Service. Climate data store (2023). URL https://cds.climate.copernicus.eu/datasets. Accessed: 2024-10-06.

[23] Buontempo, C. *et al.* The copernicus climate change service: climate science in action. *Bulletin of the American Meteorological Society* **103**, E2669–E2687 (2022).

[24] Dee, D., Obregon, A. & Buontempo, C. Are our climate data fit for your purpose? *Bulletin of the American Meteorological Society* **105**, E1723–E1733 (2024).

[25] Hersbach, H. *et al.* The era5 global reanalysis. *Quarterly Journal of the Royal Meteorological Society* **146**, 1999–2049 (2020).

[26] Hirth, L., Mühlenpfordt, J. & Bulkeley, M. The entso-e transparency platform–a review of europe's most ambitious electricity data platform. *Applied energy* **225**, 1054–1067 (2018).

[27] Staffell, I., Pfenninger, S. & Johnson, N. A global model of hourly space heating and cooling demand at multiple spatial scales. *Nature Energy* 1–17 (2023).

[28] Hofmann, F., Hampp, J., Neumann, F., Brown, T. & Hörsch, J. Atlite: a lightweight python package for calculating renewable power potentials and time series. *Journal of Open Source Software* **6**, 3294 (2021).

[29] Copernicus Climate Change Service. Climate and energy indicators for europe from 2005 to 2100 derived from climate projections (2021).

URL https://cds.climate.copernicus.eu/datasets/sis-energy-derived-projections?tab=overview. Accessed: 2024-10-06.

[30] Herrera, M. *et al.* A review of current and future weather data for building simulation. *Building Services Engineering Research and Technology* **38**, 602–627 (2017).

[31] McKinsey & Company. Transformation of europe's power system until 2050 (2010). URL https://www.mckinsey.com/~/media/mckinsey/dotcom/client_service/epng/pdfs/transformation_of_europes_power_system.ashx. Accessed: 2024-09-11.

[32] Karimi, S., Musilek, P. & Knight, A. M. Dynamic thermal rating of transmission lines: A review. *Renewable and Sustainable Energy Reviews* **91**, 600–612 (2018).

[33] Cain, M. B., O'neill, R. P., Castillo, A. *et al.* History of optimal power flow and formulations. *Federal Energy Regulatory Commission* **1**, 1–36 (2012).

[34] Ahmed, A., McFadden, F. J. S. & Rayudu, R. Weather-dependent power flow algorithm for accurate power system analysis under variable weather conditions. *IEEE Transactions on power systems* **34**, 2719–2729 (2019).

[35] Kocuk, B. *Global optimization methods for optimal power flow and transmission switching problems in electric power systems*. Ph.D. thesis, Georgia Institute of Technology (2016).

[36] Babaeinejadsarookolaee, S. *et al.* The power grid library for benchmarking ac optimal power flow algorithms. *arXiv preprint arXiv:1908.02788* (2019).

[37] Khaki, M., Musilek, P., Heckenbergerova, J. & Koval, D. *Electric power system cost/loss optimization using dynamic thermal rating and linear programming*, 1–6 (IEEE, 2010).

[38] Ahmed, A., Massier, T., McFadden, F. S. & Rayudu, R. *Weather-dependent ac power flow algorithms*, 1–8 (IEEE, 2020).

[39] Neumann, F. & Brown, T. *Heuristics for transmission expansion planning in low-carbon energy system models*, 1–8 (IEEE, 2019).

[40] ENTSO-E. Technologies for transmission system (2019). URL https://eepublicdownloads.blob.core.windows.net/public-cdn-container/clean-documents/tyndp-documents/TYNDP2018/consultation/Technical/Technologies4TS.pdf. Accessed: 2024-09-11.

[41] ENTSO-E. High temperature low sag conductors (htls) (2023). URL https://www.entsoe.eu/Technopedia/techsheets/high-temperature-low-sag-conductors-htls. Accessed: 2024-09-11.

[42] Ngoko, B., Sugihara, H. & Funaki, T. *A temperature dependent power flow model considering overhead transmission line conductor thermal inertia characteristics*, 1–6 (IEEE, 2019).

[43] Eser, P., Singh, A., Chokani, N. & Abhari, R. S. Effect of increased renewables generation on operation of thermal power plants. *Applied Energy* **164**, 723–732 (2016).

Supplementary Files

This is a list of supplementary files associated with this preprint. Click to download.

- NENERGY24102916Supplementary.pdf